Linearized inversion of scatterometric data to obtain surface profile information

Emmanuel M. Drège, MEMBER SPIE
Jeffrey A. Reed
Dale M. Byrne, MEMBER SPIE
University of Texas at Dallas
Erik Jonsson School of Engineering and Computer Science
MS EC33
Richardson, Texas 75083
E-mail: byrne@utdallas.edu

Abstract. Optical diffraction has been demonstrated to be a useful method with which to noninvasively examine materials and structures that result from lithographic processes used in the semiconductor industry to create integrated circuits. The process of inferring the geometry of the lithographically created structures from measurements of diffracted power is rather difficult, due to the highly nonlinear relationship between the properties of the diffracting structure and the diffraction measurements. To simplify this process, we describe a method that is based on determining the departures from a set of expected design values. We show that this method linearizes the otherwise highly nonlinear relationship between structure parameter values and diffraction measurements, and hence permits analyses using classical linear methods. We develop a linearized inversion technique to determine key parameters of a periodic structure from an analysis of diffraction data, and illustrate the proposed method for the retrieval of three geometrical parameters (groove depth, linewidth, and sidewall slope angle), both individually and together. We tested our method using simulated measurements of power diffracted by the grating, which were generated using rigorous coupled-wave theory. We show that our inversion algorithm predicts the correct value of these three parameters for a variety of geometrical configurations. © *2002 Society of Photo-Optical Instrumentation Engineers.*
[DOI: 10.1117/1.1416850]

Subject terms: scatterometry; diffraction; metrology; inverse problems; gratings; microlithography.

Paper 010054 received Feb. 19, 2001; accepted for publication June 11, 2001.

1 Introduction

As emphasized in the International Technology Roadmap for Semiconductors (ITRS),[1] advances in metrology are essential in maintaining adequate and affordable process latitude in the lithographic industry. Metrology not only is needed for characterizing and monitoring every processing stage, such as exposure, post-exposure bake (PEB), sillylation, and etching, but is also expected to perform in association with a seemingly ever-increasing plethora of requirements, such as being noninvasive, rapid, accurate, reliable, and *in situ*. At the same time, a combination of new chip technologies, shrinking device geometries, new process steps, major changes in materials, and different wafer sizes are conspiring to complicate the job of measuring and inspecting processed wafers.

To sustain the successful growth observed by the semiconductor industry over the last three decades, measurement science has been continuously witnessing changes. In lithographic metrology, the past decade has observed a shift from mostly imaging techniques (i.e., CD-SEM, AFM) to nonimaging schemes, such as electrical linewidth measurement[2] and more importantly, scatterometry.[3–7] The latter is an optical technique relying on diffraction to provide information about a sample surface, and can be best described as the measurement and analysis of light scattered from a surface with periodic properties. Light incident on a periodic structure (e.g., a surface relief grating), is diffracted into distinct orders, with the optical power in each order being sensitive to the geometrical characteristics of the diffracting structure as well as intrinsic properties of the materials comprising it. Conveniently, the power in each diffracted order is relatively easy to measure.

While these features make optical diffraction from surface relief gratings appealing as a monitor for lithographic processes, the extraction of relevant constitutive parameters from diffraction data can be quite cumbersome. Statistical methods such as principal component analysis,[8] discriminant analysis,[9] or partial least-square calibration,[10] as well as neural network[11,12] and nonlinear regression approaches,[13] have been proposed and tested with some success, but still possess a certain number of limitations including speed and level of accuracy. In addition, all of these methods, except for the last one, require the use of large databases that are typically generated for specific geometries.

Because lithographic processes are usually quite stringently controlled, one expects that a fabricated structure differs from its design structure by only small amounts in a limited set of parameters. We propose a technique to determine the departures from this set of expected design values. As a consequence of formulating the problem in this manner, the relationship between the parameters that describe the diffracting structure and the diffraction measurements is linearized, permitting analysis by classical linear methods. We examine the range of departures that can reasonably be

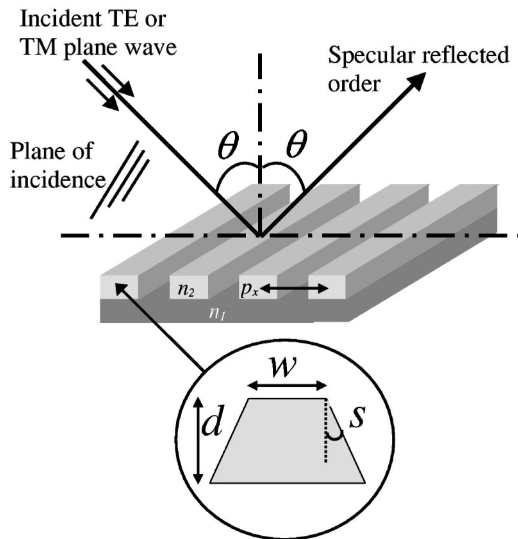

Fig. 1 Geometry of the diffraction configuration. The enlargement shows the cross section of a grating linewidth with more details.

determined for each of three parameters (groove depth, line width, and sidewall slope angle), individually and together.

In Sec. 2 we discuss how scatterometric measurements contain specific information about the diffracting structure. In Sec. 3 we present the mathematical formalism that forms the basis of subsequent analyses and examples. In Sec. 4 we show how our proposed inversion method is applied to simulated data for several different physical structures. We specifically examine the effects that polarization has on the analyses of scatterometry data. We demonstrate the ability of our proposed method to determine width, height, and sidewall slope angle of the surface relief profile, without any theoretical limitations in the absolute dimensions of those parameters. In Sec. 5 we summarize our results and establish some basic conclusions regarding the proposed inversion method, its strengths, and limitations.

2 Measurement Sensitivity

The experimental configuration that we simulate for all analyses presented is the so-called 2-θ configuration,[14] and is shown schematically in Fig. 1. The incident beam and the normal to the diffracting surface form a plane (the plane of incidence) that is perpendicular to the direction of the grooves that form the grating. In this configuration the direction of propagation of the diffracted wave (denoted by the angle θ_m) is given by the grating equation

$$\sin \theta_i + \sin \theta_m = m\left(\frac{\lambda}{d}\right), \tag{1}$$

where θ_i is the angle of incidence, θ_m is the angle of the m'th diffracted order, λ is the wavelength of the incident beam, d is the period of the grating, and m is an integer that indicates the specific diffracted order ($m=0,\pm 1,\pm 2,\cdots$). Both θ_i and θ_m are measured relative to the normal to the grating surface. In our study, we examine cases for which the incident beam is linearly polarized in either of two orthogonal linear polarization states, specifically with (1) the electric field strength, $\vec{E}$, oscillating in the plane of incidence (the TM mode, or, p polarization), or (2) the electric field strength oscillating perpendicular to the plane of incidence (the TE mode, or, s polarization). Using the 2-θ configuration, only reflected power in the zeroth order is detected ($m=0$), so that $\theta_0=-\theta_i$. This is merely a statement of the law of reflection for the undiffracted or specularly reflected order. A measurement set (scatter signature) is obtained by recording the reflected zeroth order irradiance as the incident angle is varied.

The structures studied are surface relief structures that are etched in PMMA and supported by a silicon substrate. Figures 2(a), 2(b), and 2(c) show theoretical curves for several different grating geometries for the case of incident TE polarized light. For all three graphs of Fig. 2, the grating period is $p=0.6\,\mu$m and the incident beam wavelength is $\lambda=0.6328\,\mu$m. In all simulations presented here, the refractive index used for silicon is $n=3.85-0.02i$, and for PMMA is $n=1.56-0.01i$. For the curves in Fig. 2(a), the width of the grating lines, w, is 0.3 μm, and the sidewalls are vertical (slope angle s is 0 deg). The different curves are for different groove depths, ranging from $d=0.50$ to $d=0.53\,\mu$m in increments of 5 nm. This group of curves clearly indicates that sensitivity to groove depth occurs for angular ranges from 0 to about 5 deg, from about 10 to about 30 deg, and again for angles greater than about 31 deg. These are the ranges for which the curves separate from one another as the groove depth is changed.

Figure 2(b) shows a similar set of curves for different widths of the grating lines. For the curves in Fig. 2(b), the groove depth is held fixed at a value of 0.50 μm and the sidewalls are again assumed to be vertical while the linewidth is varied from 0.30 to 0.33 μm in increments of 5 nm. Again, it is evident that certain angular ranges exist for which there appears to be sensitivity to the linewidth, but these angular ranges are not the same as those that possess sensitivity to the groove depth. Specifically, we notice very little sensitivity to linewidth for the angular range extending from 0 to 5 deg, the angular range which exhibited maximum sensitivity for groove depth. However, significant sensitivity to linewidth is apparent for incident angles greater than about 20 deg, as well as for angles between about 7 and 15 deg.

Figure 2(c) shows yet another set of curves for varying slope angles of the sidewalls. It is assumed here that both sidewalls are inclined similarly, so that if one sidewall represents an undercut profile, then the other one does also, i.e., the line profile is symmetrical. For all curves in Fig. 2(c), the linewidth at the top of the grating line is 0.3 μm and the groove depth is 0.50 μm. It is interesting to note that the curves for variation of the slope angle of the sidewalls are generally similar to those of Fig. 2(b) for variation of the linewidth.

To more clearly delineate the sensitivity as a function of incidence angle, we examine the partial derivatives of the reflectance with respect to each grating parameter (groove depth, linewidth, and sidewall slope angle), i.e., we plot $\partial R(\theta,p_i)/\partial p_i$ as a function of θ for $i=1$, 2, and 3, such that $p_1=d=$groove depth, $p_2=w=$linewidth, and $p_3=s=$sidewall slope angle. Figure 3(a) shows the partial derivatives as a function of incidence angle for a groove depth

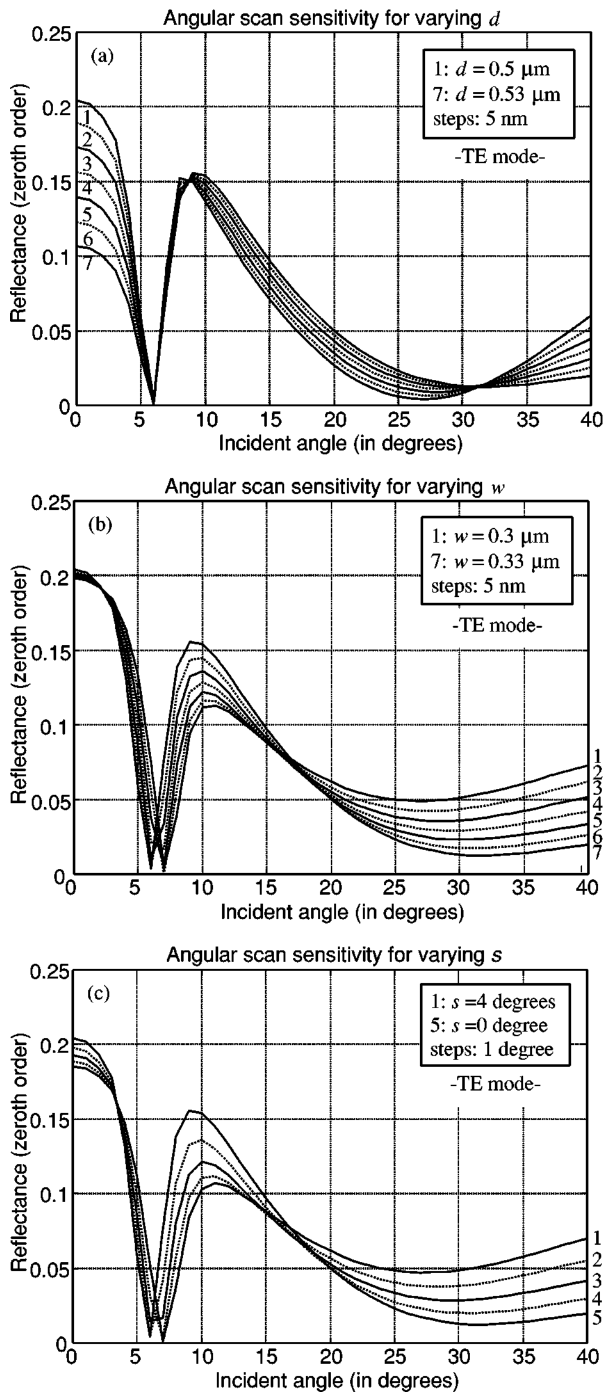

Fig. 2 TE mode angular sensitivity curves for several geometrical profile parameters: (a) groove depth variation, (b) linewidth variation, and (c) sidewall angle variation.

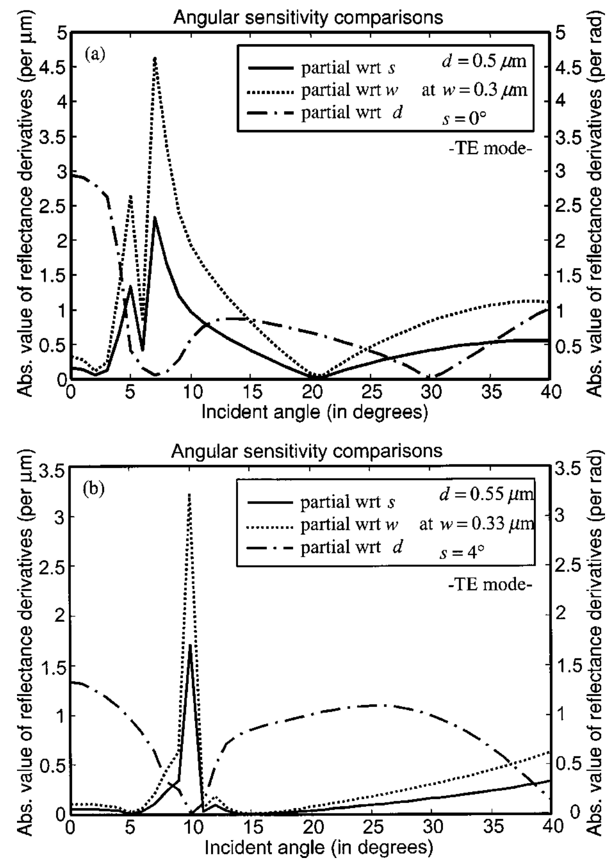

Fig. 3 TE mode angular sensitivity through partial derivatives of reflectance with respect to groove depth, line width, and sidewall angle for two different sets of parameter values.

of 0.5 μm, a linewidth of 0.3 μm, and a sidewall slope angle of 0 deg. Figure 3(b) shows the partial derivatives evaluated for $d = 0.53$ μm, $w = 0.33$ μm, and $s = 4$ deg. Both sets of curves clearly indicate the varying sensitivity that the measurements possess to the angle of incidence. In Fig. 3(a), the partial derivatives with respect to both slope angle and linewidth have sharp peaks for an angle of incidence of about 7 deg, and are nearly zero around 20 or 21 deg. This is in almost complete contrast to the derivative of reflectance with respect to groove depth, which shows a minimum in the angular range from about 6 to 8 deg, and a broad peak that extends from about 12 to nearly 30 deg. Figure 3(b) shows that if the partial derivatives were evaluated at a different location in parameter space, then the sensitivities will, in general, be different. The sharp spike that was observed in the partials with respect to both sidewall slope angle and linewidth occurs for an incidence angle of about 10 deg instead of 7 deg. Very little sensitivity for these two parameters occurs for incidence angles between about 14 and about 20 deg. In fact, the sensitivity increases only moderately for larger incidence angles. In a manner similar to the case described in Fig. 3(a), the sensitivity to groove depth is nearly zero at an incidence angle of 10 deg, where the sensitivities to the other two parameters are peaked. The sensitivity to groove depth again shows a broad peak, this time extending from about a 14-deg angle of incidence to nearly a 35-deg angle of incidence.

Figures 4(a), 4(b), and 4(c) show theoretical curves for the same grating geometries as discussed previously [see Figs. 2(a), 2(b), and 2(c)] for the case of incident TM polarized light. On comparing Figs. 2(a) and 4(a), we see that some general similarities and some differences exist in the character of the curves. For TM polarization, maximum separation between the curves having different groove depths is apparent for near normal incidence, decreasing gradually to almost no separation for an incidence angle of about 31 to 32 deg. This character is nearly identical to that

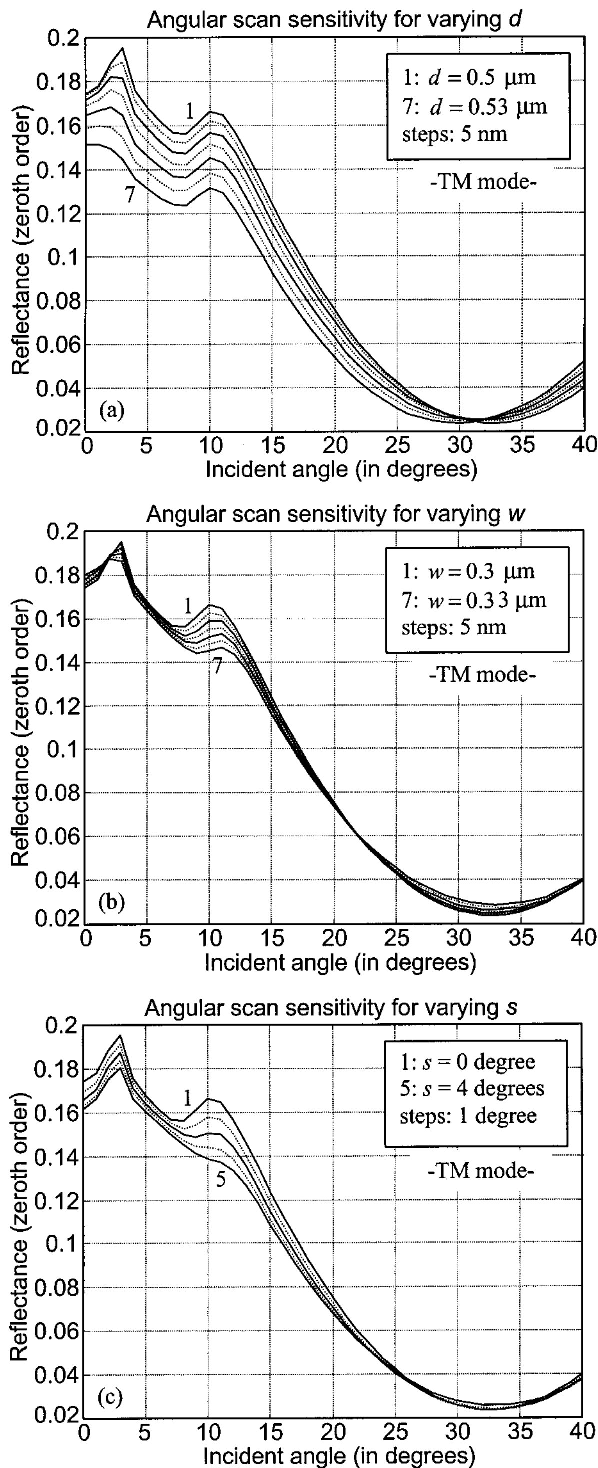

Fig. 4 TM mode angular sensitivity curves for several geometrical profile parameters: (a) groove depth variation, (b) linewidth variation, and (c) sidewall angle variation.

for TE polarization. The main difference between TE and TM polarization is that for TM polarization, there is no dip in the reflectance curve for an incidence angle of about 7 deg.

By comparing Figs. 4(b) and 2(b), we see the differences in the sensitivity to linewidth for the two polarization states. Again, the most notable difference is the lack of a dip in the reflectance curves for TM polarization. For TM polarization, the maximum separation between curves is apparent for incidence angles lying between 9 and 13 deg, which is similar to that observed for TE polarization. For incidence angles lying between about 25 and 40 deg, we notice that separation between the curves is less for TM polarization than it is for TE.

On comparing Figs. 2(c) and 4(c) showing the sensitivity of reflectance to the sidewall slope angle, we again see that the most notable difference is the lack of a near zero reflectance region for incidence angles near 7 deg for the TM polarization, and the decreased sensitivity for incidence angles ranging between 25 and 40 deg for the TM polarization.

In Figs. 2(a), 2(b), and 2(c) we see that there are small ranges of incidence angles for TE polarization in which all the curves on a given graph nearly cross one another, such as the region around 6 and 31 deg in Fig. 2(a), the region from 0 to about 4 deg and the region around 17 deg in Fig. 2(b), and the regions around 3 and 17 deg in Fig. 2(c). These stated ranges of incidence angles provide little or no information as to the parameter that is being examined, because the reflectivity measurements are not sensitive to variations in that respective parameter. This is also shown in Figs. 3(a) and 3(b) as angular regions for which the respective partial derivative is nearly zero. For TM polarization, this situation is shown in Fig. 4(a) for incidence angles of about 31 deg, in Fig. 4(b) for incidence angles of about 20 to 22 deg, and in Fig. 4(c) for incidence angles between 25 and 40 deg. These relationships between the zeroth order reflectivity and the structural parameters of groove depth, linewidth, and sidewall slope angle form the motivation for using 2-θ scatterometry to determine the structural parameters that describe the grating line profile.

3 Mathematical Formalism

In the previous section, we showed that zeroth order reflectance data are, in general, sensitive to the structural parameters that describe the grating lineshape. Therefore, we begin our formalism by approximating the measured scatterometric data by the functional form that is predicted by the rigorous coupled wave theory (RCWT).[15–18] We express this relationship as

$$R_i \approx \hat{R}_{\mathrm{RCWT}}(\theta_i, \mathbf{p}), \quad i = 1 \ldots m, \tag{2}$$

where R_i is the measurement of the reflectance at angle θ_i, $\hat{R}_{\mathrm{RCWT}}(\theta_i, \mathbf{p})$ is the theoretical value of the reflectance at that angle, assuming a set of parameter values $\mathbf{p}$, and m represents the number of angular measurements.

The success in fabricating integrated circuits of smaller and smaller dimensions is due in large part to the quality and reproducibility of the lithographic processes. Lithographic processes used to produce integrated circuits are quite stringently controlled, so that variability from wafer to wafer and batch to batch is minimized. As part of the fabrication process, it is common to include a test structure somewhere on the wafer. This test structure typically takes the form of a series of lithographically created lines and spaces—a small diffractive structure. The tacit assumption is that if this test structure possesses a profile that is close to

the desired profile, then the lithographic process is of high quality, and the actual circuitry on the wafer will function as designed. Hence, the determination of the lineshape profiles in these test gratings is a prime monitor in the fabrication of integrated circuits.

On considering that the fabrication process is so stringently controlled, it should be reasonable to expect that the lineshape profile forming the periodic structure should differ from the design structure by only small increments in a limited set of parameters. The presence of too large a departure would certainly be indicative of a flaw in the process. We therefore formulate a method to determine the departures from a set of expected design values. We define the difference between the parameter value that describes the fabricated structure and the design parameter value as

$$\Delta p_j = p_j^{(a)} - p_j^{(0)},\ \ j=1 \ldots N, \tag{3}$$

where $p_j^{(0)}$ is the design value for parameter p_j, $p_j^{(a)}$ is the parameter that describes the structure that was actually fabricated, and N represents the number of structural parameters. With the assumption that all Δp_j are small, we approximate the actual expression for the reflectances by the first two terms of a Taylor series expansion, using the design values of the parameters as starting points. We express this procedure as

$$\hat{R}_{\mathrm{RCWT}}(\theta_i, \mathbf{p}^{(a)}) \approx \hat{R}_{\mathrm{RCWT}}(\theta_i, \mathbf{p}^{(0)}) + \sum_{j=1}^{N} \left[\frac{\partial \hat{R}_{\mathrm{RCWT}}(\theta_i, \mathbf{p}^{(0)})}{\partial p_j} \right]_{p_j^{(0)}} \Delta p_j . \tag{4}$$

When Eq. (4) is substituted into Eq. (2), we obtain an approximation to the scatterometric data:

$$R_i \approx \hat{R}_{\mathrm{RCWT}}(\theta_i, \mathbf{p}^{(0)}) + \sum_{j=1}^{N} \left[\frac{\partial \hat{R}_{\mathrm{RCWT}}(\theta_i, \mathbf{p}^{(0)})}{\partial p_j} \right]_{p_j^{(0)}} \Delta p_j . \tag{5}$$

By regrouping terms, we arrive at the following expression relating the departures of parameters from their design values and differences between the measured reflectances and the expected reflectances based on the design structure. This expression becomes

$$R_i - \hat{R}_{\mathrm{RCWT}}(\theta_i, \mathbf{p}^{(0)}) = \Delta R(\theta_i) \approx \sum_{j=1}^{N} \left[\frac{\partial \hat{R}_{\mathrm{RCWT}}(\theta_i, \mathbf{p}^{(0)})}{\partial p_j} \right]_{p_j^{(0)}} \Delta p_j . \tag{6}$$

Since this expression is assumed to hold for all angles of incidence, the set of equations for the m measurement angles can be written in matrix form as

$$\Delta \mathbf{R} = \mathbf{M} \Delta \mathbf{p}, \tag{7}$$

where the elements of the matrix $\mathbf{M}$ are defined by:

$$M_{ij} = \left. \frac{\partial \hat{R}_{\mathrm{RCWT}}(\theta_i, \mathbf{p}^{(0)})}{\partial p_j} \right|_{p_j^{(0)}} . \tag{8}$$

Equation (7) is a linear system of M equations with N unknown Δp_j.

If $\mathbf{M}$ is a square matrix (number of measurements equals number of unknowns), then Δp_j can be computed by determining the inverse of $\mathbf{M}$ as given by

$$\Delta \mathbf{p} = \mathbf{M}^{-1} \Delta \mathbf{R}. \tag{9}$$

In most cases, however, the number of measurements is greater than the number of unknowns, and hence $\mathbf{M}$ is not square. This is the overdetermined problem, whose solution for Δp in this case represents the set of diffractive structure parameters that provide the best fit to the data in a least squares sense. In this case, the mathematical connection between measurements and unknowns is given by the Moore-Penrose pseudoinverse,

$$\Delta \mathbf{p} = (\mathbf{M}^{\mathbf{T}} \mathbf{M})^{-1} \mathbf{M}^{\mathbf{T}} \Delta \mathbf{R}, \tag{10}$$

where the superscript $^{\mathbf{T}}$ denotes the matrix transpose. Equations (9) and (10) indicate that our assumption of small parameter departures from their respective design values linearizes the problem. Differences between the actual reflectance measurements and those expected based on the grating design parameters are used to compute profile departures from design values.

To further evaluate the plausibility of our proposed method, we examine the magnitude of the higher power terms in the Taylor series expansion of the reflectance function. To do this we determine the reflectance as a function of incidence angle using RCWT, and then subtract our linear approximation from it. The result can be termed the residual or the remainder, which is the summation of all terms with powers higher than unity in Δp_j (including cross terms). If the remainder is near zero, then the proposed linearization quite closely resembles the actual function as computed using RCWT. Figures 5(a), 5(b), and 5(c) show the remainder term for TE polarization for the three individual parameters of groove depth, linewidth, and sidewall slope angle, while Figs. 6(a), 6(b), and 6(c) show the residuals for TM polarization for the same three parameters. Variation of the linear approximation with incidence angle is indicated in all of these graphs and gives rise to the representation in three dimensions. For each of the graphs of Figs. 5 and 6, two of the three geometrical parameters are held constant, while the other is varied. In Fig. 5(a), as an example, there is no variation in either the linewidth or the sidewall slope angle, which are held constant at 0.3 μm, and 4 deg, respectively. Only the groove depth is varied. In Fig. 5(b), only the linewidth is varied, with the groove depth and sidewall slope held constant at 0.5 μm and 4 deg, respectively, and in Fig. 5(c), only the slope angle is varied, with the groove depth and linewidth held constant at 0.5 and 0.3 μm, respectively.

All of the curves shown in Fig. 5 are relatively flat, and show most variation for small incidence angles, typically less than about 10 deg. The surface shown in Fig. 5(a) for small variation in groove depth is nearly zero for groove

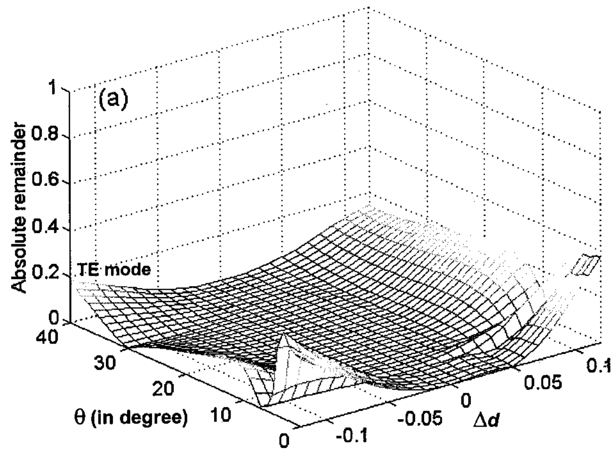

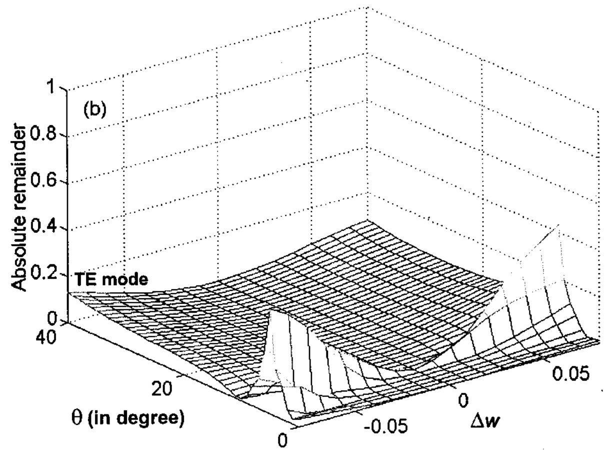

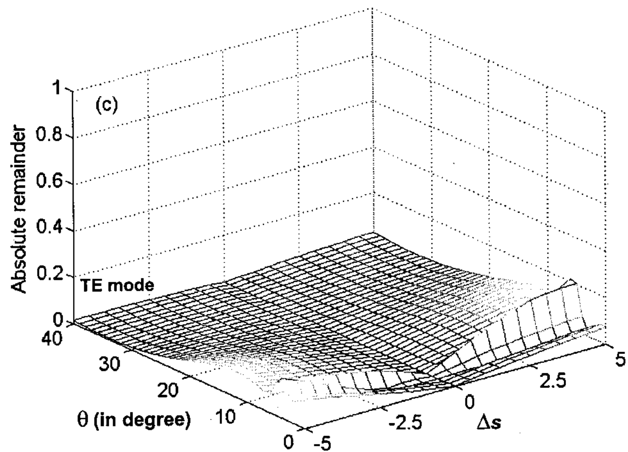

Fig. 5 TE mode angular reflectance residual after linear approximation for variation in (a) groove depth, (b) linewidth, and (c) sidewall angle.

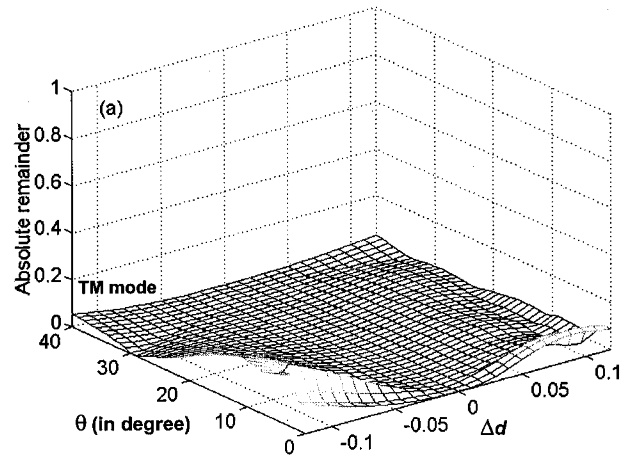

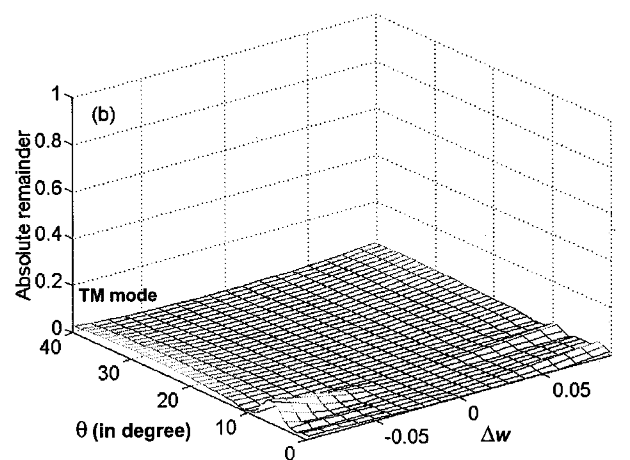

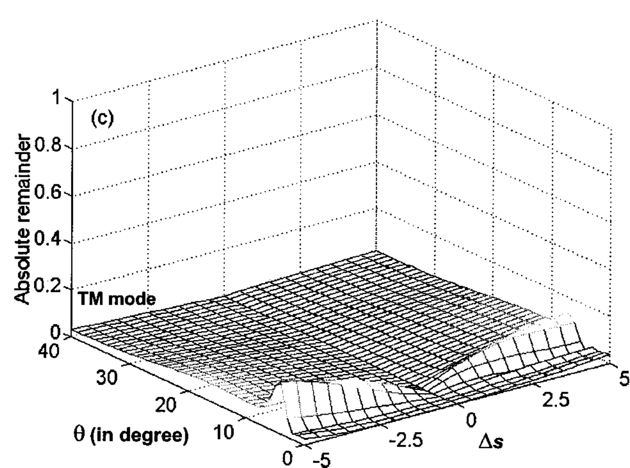

Fig. 6 TM mode angular reflectance residual after linear approximation for variation in (a) groove depth, (b) linewidth, and (c) sidewall angle.

depth variations between -0.025 and $+0.05$ μm for most angles of incidence. It is interesting to note that for an incidence angle of 30 deg, the surface is nearly zero for parameter variations between -0.12 and $+0.05$. One can conclude from these observations that our linear approximation is valid over a limited range of parameter excursions, and that these parameter variations are not the same at all angles of incidence. Generally similar statements can be made about the linewidth and slope angle surfaces of Figs. 5(b) and 5(c). The surface shown in Fig. 5(c) appears to be the flattest surface of the three, indicating that our linear approximation should hold for a wide range of slope departures for most angles of incidence.

Statements similar to those made about the surfaces in Figs. 5(a), 5(b), and 5(c) can also be made about the surfaces shown in Figs. 6(a), 6(b), and 6(c) for TM polarization. However, one observes that the surfaces for TM polarization are smoother and closer to zero for most angles

of incidence and for larger departure values than those for TE polarization. Except for the groove depth variation, the largest variation is limited to incidence angles less than about 10 deg. This indicates that our linear approximation appears to be more valid for TM than for TE polarization.

Our assumption is that if the parameters of the grating that was actually produced differed only slightly from those of the design structure, then the parameter departures calculated using Eqs. (9) or (10) would produce a structure that exactly reproduced the measured data. However, in any experimental situation, reflectance data may be produced by parameter values that depart from the design values by an amount (albeit small) that exceeds the range of validity of our linear approximation. Hence, because the relationship between parameter values and reflectance measurements is, in general, highly nonlinear, our linear approximation might not produce the correct departure values even for moderately small parameter departures. To account for this somewhat inevitable situation, we make the inversion process iterative by calculating departures and then updating the parameter values, to be used as the starting point for the computation of new departure values. This procedure continues until no further changes in the parameter values occur. Each step is equivalent to making a new starting point for the Taylor series expansion. For each iteration through the process, RCWT is used to connect the measurements to the reflectance differences.

4 Inversion Results and Interpretations for Simulated Data

To evaluate the performance of our linearized inversion process, we simulated diffraction measurements using the RCWT. Reflectance as a function of incidence angle for a given polarization state was computed for an assumed design profile. We then simulated reflectance data by computing the reflectance as a function of incidence angle for a profile that differed from the design profile by a specified amount in one or more of the three parameters previously discussed. In this section, we describe the results when this simulated data were used as input to our linearized inversion procedure.

4.1 *Single Parameter Inversions*

Figure 7(a) shows the design profile and a groove depth that is greater than the design value by 10%. Figure 7(b) shows both the simulated reflectance data for the simulated actual structure (the one that has a groove depth 10% greater than the design) as well as the reflectance data that would be produced by the design profile for incidence angles from 0 to 40 deg. The simulated actual reflectance is generally similar in character to the design reflectance curve, but has distinct differences. On subjecting the simulated actual data to our algorithm, we found that after only two iterations the groove depth parameter converged to the actual groove depth that produced the simulated data.

We then conducted similar simulated experiments for a geometry that differed from the design geometry only in the width of the top of the structure by 10% as seen in Fig. 8(a), and a geometry that differed from the design geometry by 10% only in the slope of the sidewalls, as illustrated in Fig. 9(a). Simulated data were generated for each of these cases and analyzed using our algorithm. Figure 8(b) shows

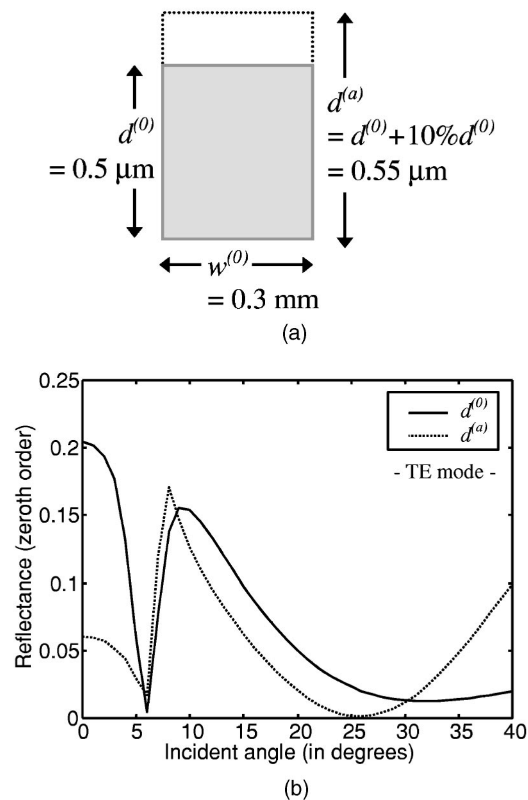

Fig. 7 (a) Cross section of a grating profile showing the actual and design depths, and (b) their respective angular reflectances for the TE mode.

both the reflectance data for the simulated actual structure (the one that has a top linewidth 10% greater than the design) as well as the reflectance data that would be produced by the design profile for incidence angles from 0 to 40 deg. Again, we observe that the data for the simulated actual structure has a generally similar character to the reflectance curves for the design, although the curves are still noticeably different. When these curves were subjected to our algorithm, we found that after only three iterations, the width parameter converged to the value of the simulated actual structure.

Figure 9(b) shows both the reflectance data for the simulated actual structure (the one that has a sidewall slope angle 10% greater than the design) as well as the reflectance data that would be produced by the design profile for incidence angles from 0 to 40 deg. We see that for this case, the curves are very similar, differing only by small amounts, primarily for incidence angles greater than about 15 deg. When this data set was used as input to our algorithm, the sidewall slope parameter converged to the simulated actual value in three iterations also.

Figure 10 shows convergence characteristics of each parameter as it progresses from its initial to its final value. The percent difference between the actual parameter value and the one that resulted from each iteration for each of the three cases is plotted as a function of iteration step. We see that the groove depth and grating width each converged to the correct value monotonically, while the slope angle incurred a slight oscillation, overshooting the correct value

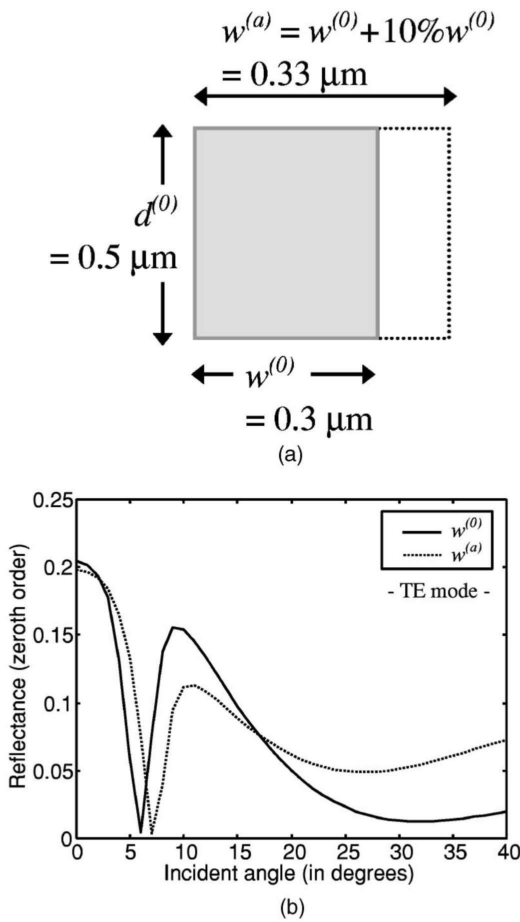

Fig. 8 (a) Cross section of a grating profile showing the actual and design linewidths, and (b) their respective angular reflectances for the TE mode.

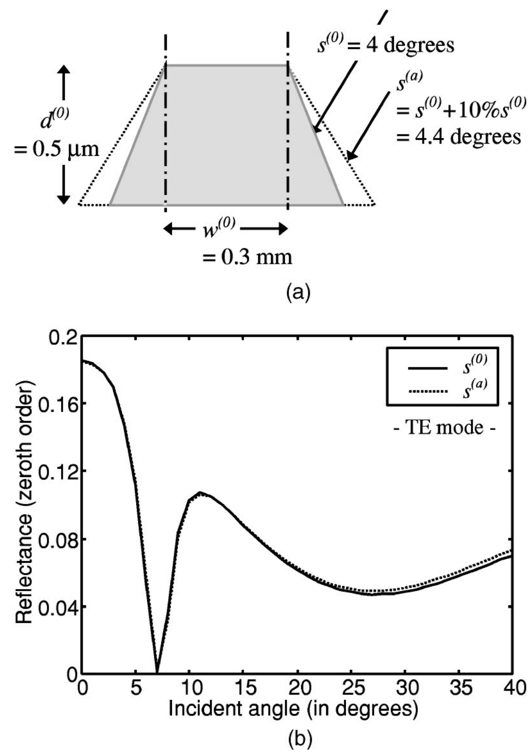

Fig. 9 (a) Cross section of a grating profile showing the actual and design sidewall angles, and (b) their respective angular reflectances for the TE mode.

very slightly after the first iteration. Nonetheless, each parameter converged to the correct parameter value. If we reexamine the reflectance curves shown in Figs. 7(b), 8(b), and 9(b) that correspond to the simulated data for each of the three cases, we find that although the respective parameter differed by 10% in each case, the resulting effect on the reflectance data was quite different. A 10% difference from the design value for groove depth and linewidth produced a reflectance curve that was noticeably different than that for the design value. In contrast, a 10% difference in sidewall slope angle produced a reflectance curve that was very similar to the reflectance curve corresponding to the design value. In all cases, it can be said that the simulated actual data had generally similar character to the design data. Hence, we would not expect dramatic differences in the convergence character of the three parameters. However, the specific nature of the convergence results and the effect of a specified percentage departure of a given parameter on the reflectance curve is dependent on the design value of that parameter (as well as the amount of departure), and hence, these convergence results should not be considered to be an inherent property of the inversion algorithm.

4.2 *Multiparameter Inversions*

In the preceding section, we illustrated the recovery of a single structural parameter using our linearized inversion method and found that it was capable of determining the correct parameter value in relatively few iterations. To further examine this method, we applied our technique to determine multiple parameters simultaneously. We conducted simulated experiments for geometries in which all three parameter values differed from the design geometry values. For this illustration, all parameters were larger than their

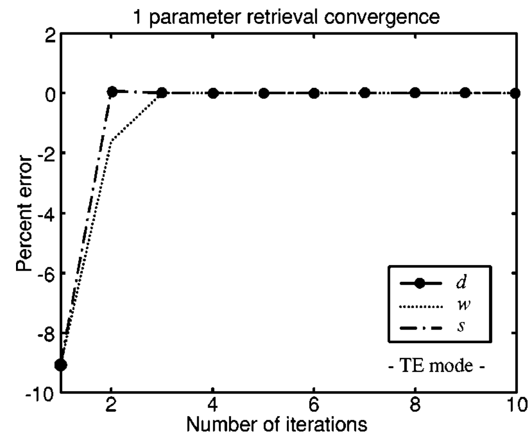

Fig. 10 Convergence curves for single parameter retrieval [$d^{(0)} = 0.5\ \mu$m, $w^{(0)} = 0.3\ \mu$m, $s^{(0)} = 4$ deg] in the TE mode. The percent error between retrieved and actual values is plotted as a function of number of iterations.

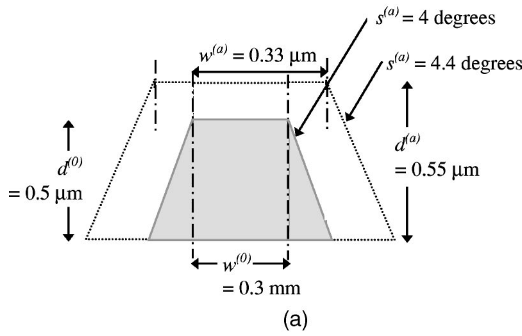

(a)

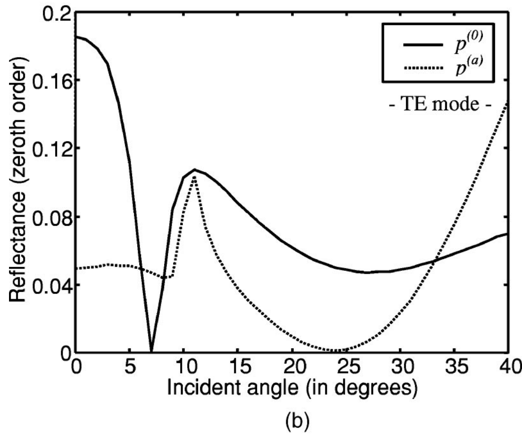

(b)

Fig. 11 (a) Cross section of a grating profile showing the actual and design parameters, and (b) their respective angular reflectances for the TE mode.

respective design parameter by 10%. Simulated data were generated for the profile geometry that is shown in Fig. 11(a). The corresponding reflectance curve that would be produced by this geometry is shown in Fig. 11(b). The reflectance curve that would have been produced by the designed profile is shown for reference. Not only do the two curves differ rather dramatically, they have generally dissimilar character. The results of using our linearized algorithm to process this simulated data are summarized by the convergence curves shown in Fig. 12. The nature of these curves is rather different from the convergence curves shown in Fig. 10. We see that the convergence of groove depth is monotonic, while the sidewall slope angle parameter oscillates significantly before converging to its final value, and the linewidth parameter diverges before finally converging to its final value. It should be remembered that all three parameters varied during each iteration. In spite of the highly oscillatory nature of the sidewall slope parameter, it still converged to the correct value, as did the other two parameters, in only seven iterations.

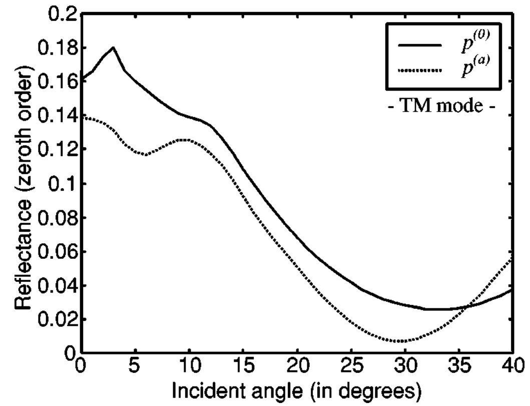

Fig. 13 Angular reflectances for the TM mode corresponding to the actual and design parameters as defined in Fig. 11(a).

All simulations previously discussed assumed that the incident light was linearly polarized in the TE mode. To determine the effects of the polarization state, we simulated reflectance data for the TM polarization state. The geometry of this structure is the same as that shown in Fig. 11(a). The TM mode simulated actual reflectance curve is shown in Fig. 13, along with the TM mode reflectance curve corresponding to the design structure. As can be seen, there is a general similarity in character between the two reflectance curves; nevertheless, the curves are appreciably different. Figure 14 shows the convergence curve for each of the three parameters. As in the previous cases, all three parameters converged to the correct parameter value. However, on comparing this set of convergence curves with that

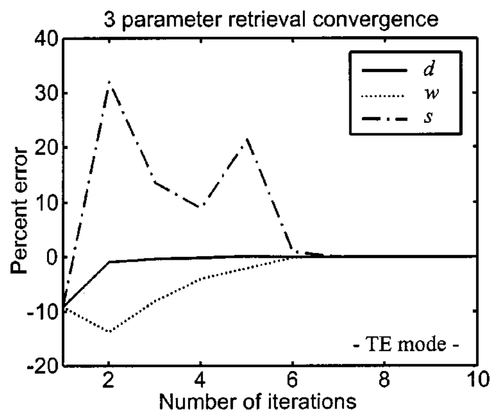

Fig. 12 Convergence curves for three parameter retrieval [$d^{(0)}=0.5\,\mu$m, $w^{(0)}=0.3\,\mu$m, $s^{(0)}=4$deg] in the TE mode. The percent error between retrieved and actual values is plotted as a function of number of iterations.

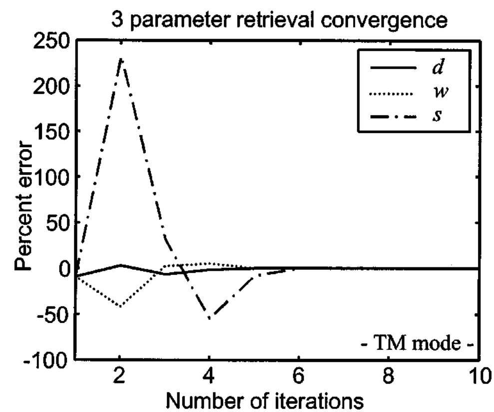

Fig. 14 Convergence curves for three parameter retrieval [$d^{(0)}=0.5\,\mu$m, $w^{(0)}=0.3\,\mu$m, $s^{(0)}=4$deg] in the TM mode. The percent error between retrieved and actual values is plotted as a function of number of iterations.

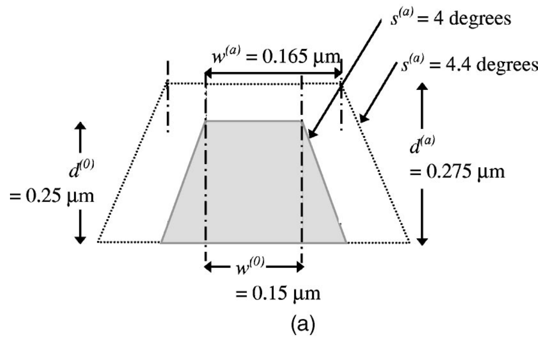

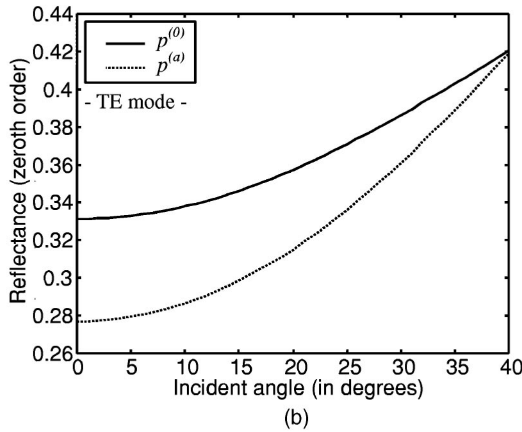

Fig. 15 (a) Cross section of a grating profile showing the actual and design parameters, and (b) their respective angular reflectances for the TE mode.

for the three-parameter TE mode case, a dramatic difference is quite apparent. For the TM mode case, none of the three parameters converges monotonically to the final result. In fact, all three parameters oscillate above and below their correct values before convergence is attained. Before its convergence, the slope angle parameter varies between an overcut and an undercut profile, but still converges to the correct value.

All of the previous simulations were based on a grating geometry that had a period of 0.6 μm, a linewidth of 0.3 μm, and a groove depth of 0.5 μm. To determine if the grating geometry could be scaled to a smaller value without similarly scaling the wavelength, we simulated reflectance data for a grating that was one-half the size of those previously described. The geometry for this grating is shown in Fig. 15(a). The period is 0.3 μm, the linewidth is 0.15 μm, the groove depth is 0.25 μm, and the sidewall slope angle is 4 deg. The simulated reflectance data for this grating (assuming the incident wave was polarized in the TE mode) are shown in Fig. 15(b), along with the simulated reflectance that would be produced by a grating for which each parameter value was increased by 10%. As shown in Fig. 15(b), the two grating geometries would produce reflectance curves that differ substantially from one another. These reflectance curves were processed using our linearized approach, with the result that after six iterations, each parameter value had converged to its correct value. Figure 16 shows the convergence curves for each of the three parameters, and indicates that, although the grating structure simulated had dimensions that were one-half those of the

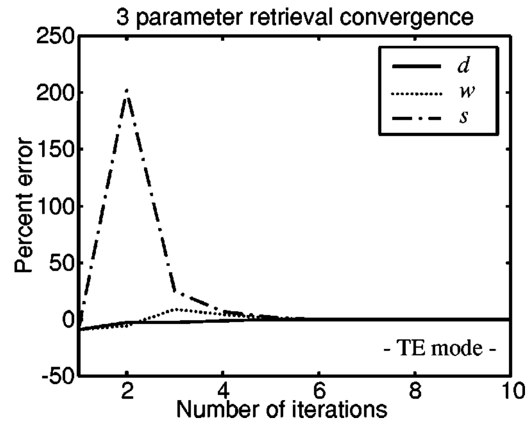

Fig. 16 Convergence curves for three parameter retrieval [$d^{(0)}=0.5\ \mu$m, $w^{(0)}=0.3\ \mu$m, $s^{(0)}=4$ deg] in the TE mode. The percent error between retrieved and actual values is plotted as a function of number of iterations.

previous simulated gratings, the nature of the convergence was essentially the same as that for the original grating geometry.

We also simulated the case in which the incident radiation was polarized in the TM mode. The simulated actual reflectance data for the TM mode (assuming that each parameter was increased by 10% from its design value) is shown in Fig. 17, along with the reflectance data that would be produced by the design structure. We see that these two curves are similar in nature but still differ from one another. Again, these reflectances were processed using our algorithm, and again, all three parameters converged to their respective, correct values. The convergence is summarized in Fig. 17. As for the TE mode case, all three parameters oscillated prior to their convergence, with the sidewall slope angle parameter oscillating with the largest amplitude.

As seen in Figs. 12, 14, 16, and 18, the slope parameter experiences a large error before converging to the correct value. We have also observed this behavior in test cases other than those reported here. This behavior can be explained by again referring to Figs. 2 and 4, where we showed that the apparent sensitivity to all three geometric

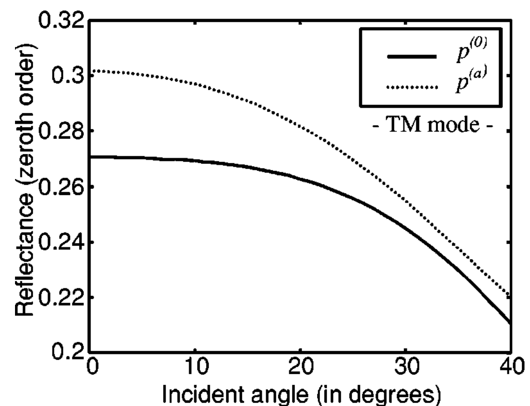

Fig. 17 (a) Cross section of a grating profile showing the actual and design parameters, and (b) their respective angular reflectances for the TM mode.

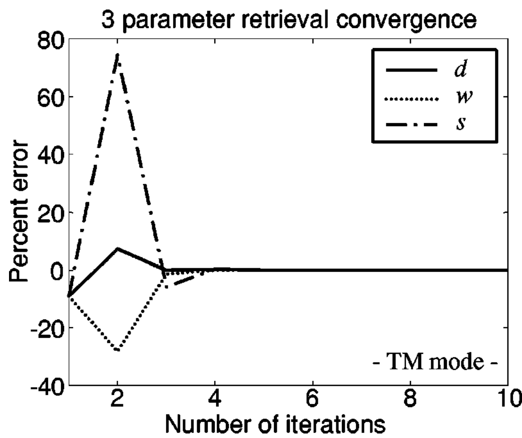

Fig. 18 Convergence curves for three parameter retrieval [$d^{(0)} = 0.5\,\mu$m, $w^{(0)} = 0.3\,\mu$m, $s^{(0)} = 4$deg] in the TM mode. The percent error between retrieved and actual values is plotted as a function of number of iterations.

parameters was approximately the same in magnitude (although varying with angle of incidence). A more careful investigation of the reflectance profiles indicates that significantly larger fractional changes in the slope were required to produce variations in reflectance similar to those produced by fractional changes in either width or depth. The implication is that there is relatively less sensitivity in reflectance measurements to slope than to either linewidth or groove depth. The result is that during the linear inversion process, more weight is given to fitting the data by appropriate choice of linewidth and groove depth, and relatively less weight to the specific value of slope. Statistically, most of the variance between reflectance data and the fitted curve is accounted for by nearly correct values for the width and depth, while the slope accounts for only a small fraction of the variance. Therefore, as our proposed iterative process proceeds, the width and depth converge to their correct values with minimal oscillation, while the slope converges to its correct value in a much more erratic fashion.

5 Summary and Conclusions

We have introduced a new approach to the inverse problem of determining surface relief profile information from scatterometric data. This approach is based on the fact that microlithographic processes produce structures whose shapes are very close to the design shapes. When this fact is modeled mathematically, a Taylor series expansion (retaining only the first two terms) produces a linear relationship between departures in parameter values (actual value minus design value) and departures in reflectance values (actual reflectance minus expected reflectance from the design structure). The departure values can conceptually be determined from the reflectance difference data by a direct matrix inversion. However, a direct matrix inversion would not be expected to produce the exact parameter departures because of the approximation arising from the truncation of the Taylor series expansion. To overcome this inherent limitation, we propose an iterative procedure in which we use the previously computed departures to compute a set of new refined parameter values. This process continues until no further changes in parameter values occur.

In this study, we have considered a general trapezoidal surface relief structure, parameterizing it by depth, width, and sidewall slope angle. Using the rigorous coupled wave theory, we have demonstrated that zeroth order reflectance data are angularly sensitive to these three parameters in varying amounts. These observations confirm that diffraction measurements from periodic structures can be used in a metrology concept to determine the characteristics of a microlithographic process, as has been discussed previously in the literature.[3,5,6]

To demonstrate how our proposed linear technique can be applied to determine the three parameters that were used to define the surface relief geometry, we conducted a series of numerical experiments. We simulated reflectance data for structures that differed from the design geometry in only a single parameter by 10%. Independent of which parameter departed from its design value, our technique was able to recover the actual parameter value with no error in less than seven iterations. To further demonstrate the potential of our technique, we generalized the parameter search to simultaneously seek departures in all three parameters. To illustrate the ability of our technique to retrieve multiple parameters, reflectance data for both TE and TM polarizations for two different surface relief geometries were generated. In each of those four cases, for which the actual parameter values differ from their respective design values by $+10\%$, our technique converged to the actual parameters, again with no error and in less than seven iterations.

Because the method proposed here is based on a direct relationship between measured reflectances and parameter values, it eliminates the need to create a large database which comparisons are made. Therefore, this method should be faster and also more flexible, in that it can be used to analyze widely differing structures. Although we show only examples of one generic type of surface relief geometry (trapezoidal), the concept is applicable to a more general class of geometrical shapes that can be described by additional parameters. In principal, one can describe an arbitrarily complex shape defined by N parameters; however, zeroth order reflectance measurements may not be very sensitive to all of these N parameters. For more complex geometries, it becomes important to analyze the information contained in the measurement set, so as to estimate the number of independent and sensitive parameters that can be derived from the data. Hence, one needs to exploit the observations drawn in Sec. 2 about the specific nature of the sensitivity of the scatterometric data to the geometry of the structure and to the polarization of the incident radiation. Furthermore, sensitivity to wavelength in the context of spectroscopic scatterometry[19,20] can also be introduced.

Based on our results, we feel that the linearized approach presented here could easily be used as a method to analyze scatterometric data collected in real time, thus making it attractive for in-line, and possibly complete batch, wafer inspection.

References

1. Semiconductor Industry Association, *International Technology Roadmap for Semiconductors*, 1999 ed., International SEMATECH, Austin, TX (1999).

2. L. Capodieci, R. Subramanian, B. Rangarajan, W. D. Heavlin, J. Li, D. A. Bernard, and V. V. Boksha, "Novel methodology for postexposure bake calibration and optimization based on electrical linewidth measurement and process metamodeling," *J. Vac. Sci. Technol. B* **16**(6), 3752–3758 (1998).
3. E. M. Drege and D. M. Byrne, "Lithographic process monitoring using diffraction measurements," *Proc. SPIE* **3998**, 147–157 (2000).
4. C. J. Raymond, M. R. Murnane, S. L. Prins, S. Sohail, H. Naqvi, J. R. McNeil, and J. W. Hosch, "Multiparameter grating metrology using optical scatterometry," *J. Vac. Sci. Technol. B* **15**(2), 361–368 (1997).
5. J. Bischoff, J. W. Baumgart, J. J. Bauer, and H. Truckenbrodt, "Light scattering based micrometrology," *Proc. SPIE* **2775**, 251–262 (1996).
6. H. P. Kleinknecht and H. Meier, "Linewidth measurement on IC masks and wafers by grating test patterns," *Appl. Opt.* **19**(4), 525–533 (1980).
7. S. S. H. Naqvi, J. R. McNeil, R. H. Krukar, and K. P. Bishop, "Scatterometry and the simulation of diffraction-based metrology," *Microlithogr. World* **2**(3), 5–16 (1993).
8. K. P. Giapis, R. A. Gottscho, L. A. Clark, J. B. Kruskal, D. Lambert, A. Kornblit, and D. Sinatore, "Use of light scattering in characterizing reactively ion etched profiles," *J. Vac. Sci. Technol. A* **9**(3), 664–668 (1991).
9. R. Krukar, A. Kornblit, L. A. Clark, J. Kruskal, D. Lambert, E. A. Reitman, and R. A. Gottscho, "Reactive ion etching profile and depth characterization using statistical and neural network analysis of light scattering data," *J. Appl. Phys.* **74**(6), 3698–3706 (1993).
10. S. S. H. Naqvi, R. H. Krukar, J. R. NcNeil, J. E. Franke, T. M. Niemczyk, D. M. Haaland, R. A. Gottscho, and A. Kornblit, "Etch depth estimation of large-period silicon gratings with multivariate calibration of rigorously simulated diffraction profiles," *J. Opt. Soc. Am. A* **11**(9), 2485–2493 (1994).
11. I. Kallioniemi, J. Saarinen, and E. Oja, "Characterization of diffraction gratings in a rigorous domain with optical scatterometry: hierarchical neural-network model," *Appl. Opt.* **38**(28), 5920–5930 (1999).
12. N. George and S.-G. Wang, "Neural networks applied to diffraction-pattern sampling," *Appl. Opt.* **33**(14), 3127–3134 (1994).
13. M. Lee, "High-speed analysis of surface topography on semiconductor wafers by optical diffractive techniques," Doctoral dissertation, University of Michigan (1999).
14. C. J. Raymond, M. R. Murnane, S. S. H. Naqvi, and J. R. McNeil, "Metrology of subwavelength photoresist gratings using optical scatterometry," *J. Vac. Sci. Technol. B* **13**(4), 1484–1495 (1995).
15. M. G. Moharam and T. K. Gaylord, "Three-dimensional vector coupled-wave analysis of planar-grating diffraction," *J. Opt. Soc. Am. A* **73**(9), 1105–1112 (1983).
16. T. K. Gaylord and M. G. Moharam, "Analysis and applications of optical diffraction by gratings," *Proc. IEEE* **73**(5), 894–937 (1985).
17. S. Peng and G. M. Morris, "Efficient implementation of rigorous coupled-wave analysis for surface relief gratings," *J. Opt. Soc. Am. A* **12**(5), 1087–1096 (1995).
18. N. Chateau and J. Hugonin, "Algorithm for the rigorous coupled-wave analysis of grating diffraction," *J. Opt. Soc. Am. A* **11**(4), 1321–1331 (1994).
19. N. Jakatdar, X. Niu, J. Bao, C. Spanos, S. Yedur, and A. Deleporte, "Phase profilometry for the 193 nm lithography gate stack," *Proc. SPIE* **3998**, 116–124 (2000).
20. B. K. Minhas, S. A. Coulombe, S. S. H. Naqvi, and J. R. McNeil, "Ellipsometric scatterometry for the metrology of sub-0.1-mm-linewidth structures," *Appl. Opt.* **37**(22), 5112–5115 (1998).

Emmanuel M. Drège graduated in 1994 with master's degrees in material engineering (ESIREM) and physics (University of Burgundy), France. He initially came to the University of Texas at Dallas School of Human Development to conduct research on face recognition using neural networks combined with pre-processing techniques such as wavelet and Hough transforms. He returned to France to serve one year of military duty, after which he returned to UTD to pursue the PhD in electrical engineering. He received the MSEE degree in 1999, and is currently pursuing the PhD in electrical engineering at UTD. His dissertation topic concerns the inversion of scatterometric data to determine lithographic profiles, and the design of scatterometric and ellipsometric instrumentation.

Jeffrey A. Reed graduated from the University of Virginia in 1983 with a BA in astronomy/physics. After studying astronomy at the University of Florida, he transferred to the School of Business Management at the University of Texas at Dallas, where he obtained an MBA in 1987. Jeff returned to UTD to study physics and received his MS and PhD in physics in 1989 and 1997, respectively. His dissertation topic centered around the modeling of frequency selective surfaces with multiple periodic elements. Jeff is currently a research associate at UTD, and consults with Optical Switch Corporation of Richardson, Texas.

Dale M. Byrne received the BS and MS degrees in physics from Florida Institute of Technology and the MS and PhD degrees in optical sciences from the University of Arizona Optical Sciences Center in 1976 and 1978, respectively. He worked at United Technologies Research Center in West Palm Beach, Florida and at LTV Corporation in Dallas, Texas before joining the faculty of the University of Texas at Dallas in 1987. He is currently an associate professor in electrical engineering and physics at UTD. His current research interests include a wide variety of optical inverse problems and the development of optical instrumentation and devices for ellipsometry and scatterometry.